Supplementary Information (SI) for Journal of Materials Chemistry A.

Electronic supplementary information

# Electrically conductive MOF@carbon foam composites for atmospheric water harvesting through internal joule heating and light irradiation

Lasse Wegner,[a] Philipp Schadte,[b] Ravi Sharma,[c] Carde Reimerdes,[a] Rainer Adelung,[b,d] Joeri F.M. Denayer,[c] Leonard Siebert,[b,d,e] and Norbert Stock*[a,d]

[a] Institute for Inorganic Chemistry, Kiel University, Max-Eyth Straße 2, 24116 Kiel, Germany.

[b] Functional Nanomaterials, Department of Materials Science, Kiel University, 24143 Kiel,

Germany; Kiel

[c] Department of Chemical Engineering, Vrije Universiteit Brussel, Pleinlaan 2, 1050 Brussels, Belgium

[d] Kiel Nano, Surface and Interface Science (KiNSIS), Kiel University, 24118 Kiel, Germany

[e] Centre for Surface Chemistry and Catalysis, KU Leuven – University of Leuven, Celestijnenlaan 200F, B-3001 Leuven, Belgium

Table of contents

## Description of the 3D printed casing for BT measurements

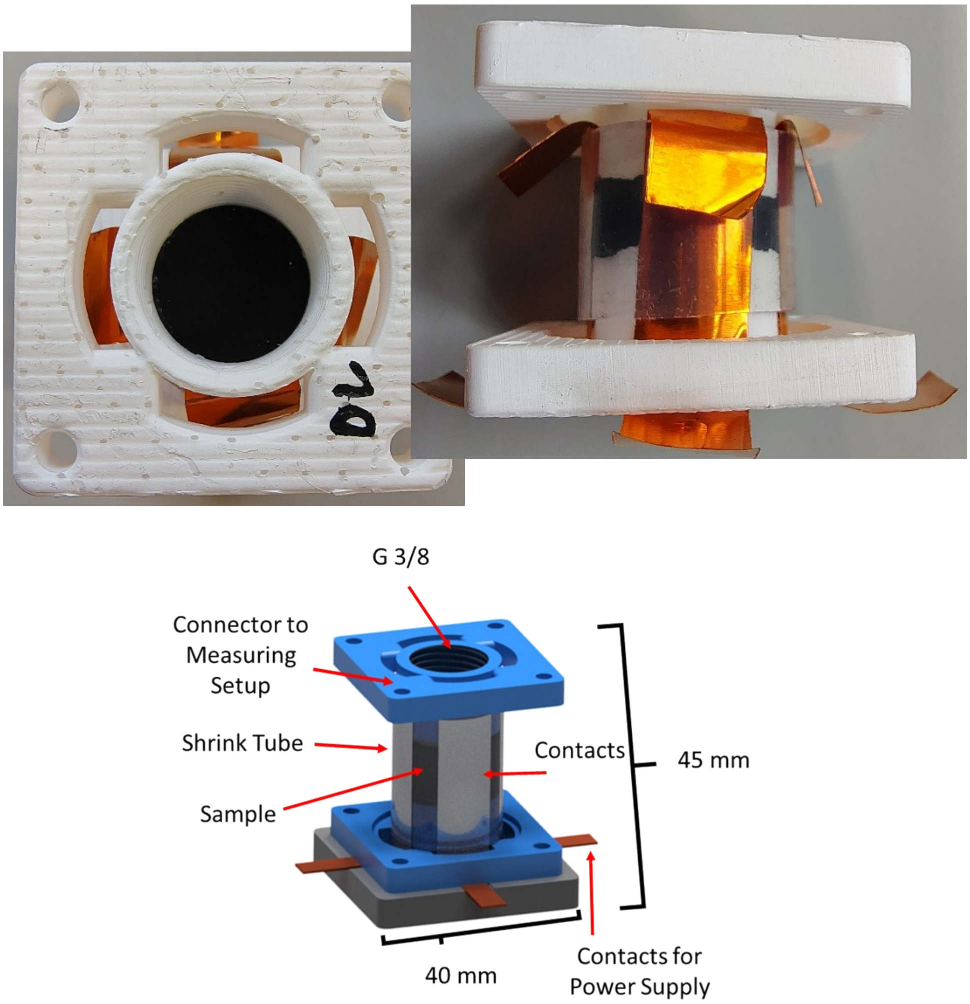

**Figure S1:** Top: Photographs of the 3D printed polymer casing with the cylindrical sample and the copper contacts used for the BT measurements before the infiltration of the MOF particles. Bottom: A sketch of the setup including the dimensions.

## Breakthrough experiments

Breakthrough curves were obtained by plotting the outlet concentration ($C/C_0$) versus time. The adsorption capacity ($q_i$) of each component was calculated via a mass balance over the column according to:

$$q_i = \frac{\left(F_{feed} \cdot \tau_{ST,i} - \varepsilon \cdot V\right) . \, x_{feed,i} \cdot \rho_f}{m_{ads}} \qquad (1)$$

with $F_{feed}$, $\tau_{ST,i}$, $\varepsilon$, $V$, $m_{ads}$, $x_{feed,i}$, and $\rho_f$ denoting the volumetric feed flow rate (ml/min), the average breakthrough time of component *i* (min), the bed porosity, total column volume (ml), the mass of the adsorbent (g), the mass fraction of the component *i* in the feed mixture (g/g), and fluid density (g/ml).

The average breakthrough time was calculated from equation 2:

$$\tau_{ST,i} = \int_0^\infty \left(1 - \frac{c_i}{c_{o,i}}\right) d\,t \qquad (2)$$

with $c_i$ and $c_{o,i}$ representing the column outlet concentration and the feed concentration.

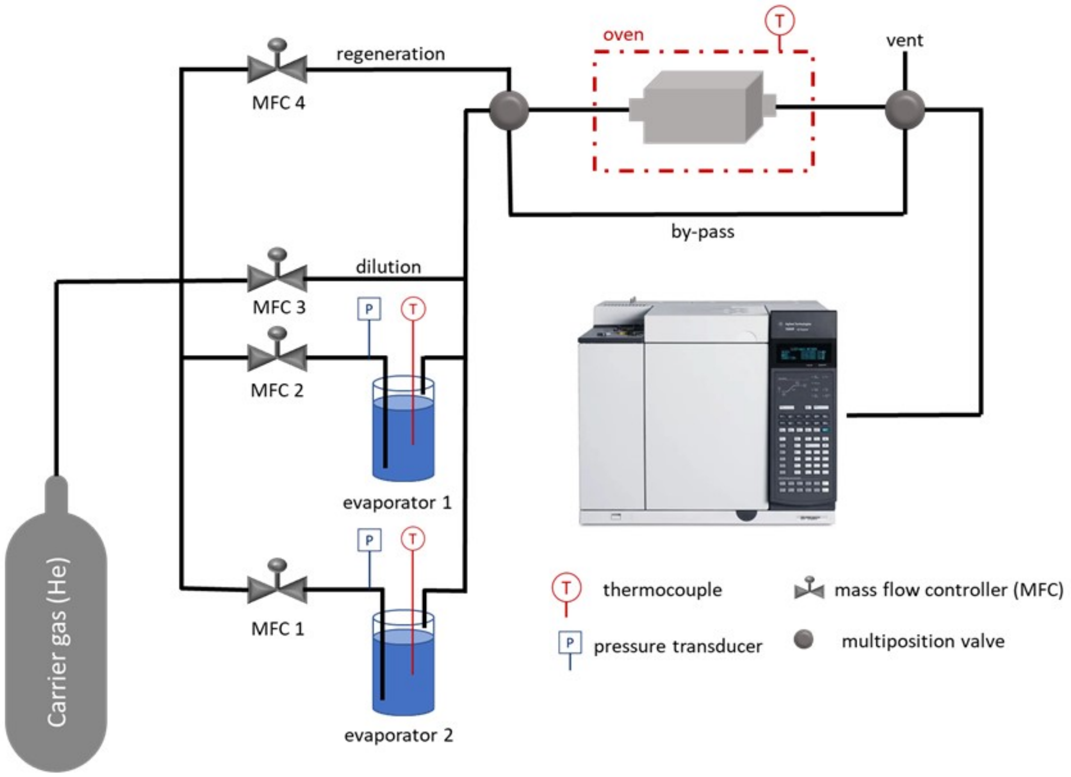

**Figure S2:** Schematic of the experimental setup to perform vapor phase breakthrough experiments. Helium (He) as carrier gas is sent through one or both evaporators to obtain a vapor stream. This vapor stream can further be diluted using another mass flow controller (MFC 3). The column is kept in a temperature-controlled oven and the effluent stream is analysed by GC. The adsorbent can be regenerated in-situ under continuous flow of carrier gas (He) by heating the column oven.

The above equations are valid only under the assumptions that no change in fluid flow rate due to adsorption is observed. The adsorbate density is also assumed constant all over the column and same as feed mixture density. It also indicates that (for vapor systems) a negligible pressure drop over the adsorbent bed is assumed, considering the structured form.

For vapor phase separation, considering the total mixture pressure at the column inlet, and the average of the total pressure for the two evaporators, the equation 1 was rewritten as:

$$q_i = \frac{\left(\dot{n}^{mix}_{tot} \cdot \tau_{ST,i} - \frac{\varepsilon V . P^{mix}_{tot}}{R . T_{ex}}\right) \cdot y^{mix}_{i}}{m_{ads}} \tag{3}$$

where $\dot{n}^{mix}_{tot}$ is the molar flow rate of the mixture (mmol/min), ' $P^{mix}_{tot}$ is the total pressure of the mixture (Pa), R is the ideal gas law constant, $q_i$ is the amount adsorbed (mmol/g), and $T_{ex}$ is the experimental temperature (K) and,

$$\tau_{ST,i} = \int_0^{\infty} \left(1 - \frac{y^{outlet}_{i}}{y^{mix}_{i}}\right) d\,t \tag{4}$$

Furthermore, a correction is needed for the dead volume of the system. This correction was made using the dead volume, $V_d = 3.5 \cdot 10^{-6}$ m$^3$, determined by Gelin () and is used as follows

$$\tau_{ST,corrected} = \tau_{ST,i} - \frac{V_d}{F_{tot}} \tag{5}$$

$F_{tot}$ is the total flow rate (m$^3$/s).

For single component adsorbate, the equation 3 can be simplified to the following:

$$q_i = \frac{F_{tot} \cdot y_{i,in} \cdot \tau_{ST,correted} \cdot MW_i \cdot P_{st}}{m_{ads} \cdot RT_{st}} \tag{6}$$

$P_{st}$ is the standard pressure (Pa), $T_{st}$ is the standard temperature (K), $y_{i,in}$ is the inlet mole fraction of adsorbate, i and $MW_i$ is the molar weight of adsorbate, i (g/mol).

The breakthrough curves of the pristine carbon foam were measured with a helium stream with a relative humidity of 20 % and 40 % to establish a baseline for the performance of the composites (Figure S3).

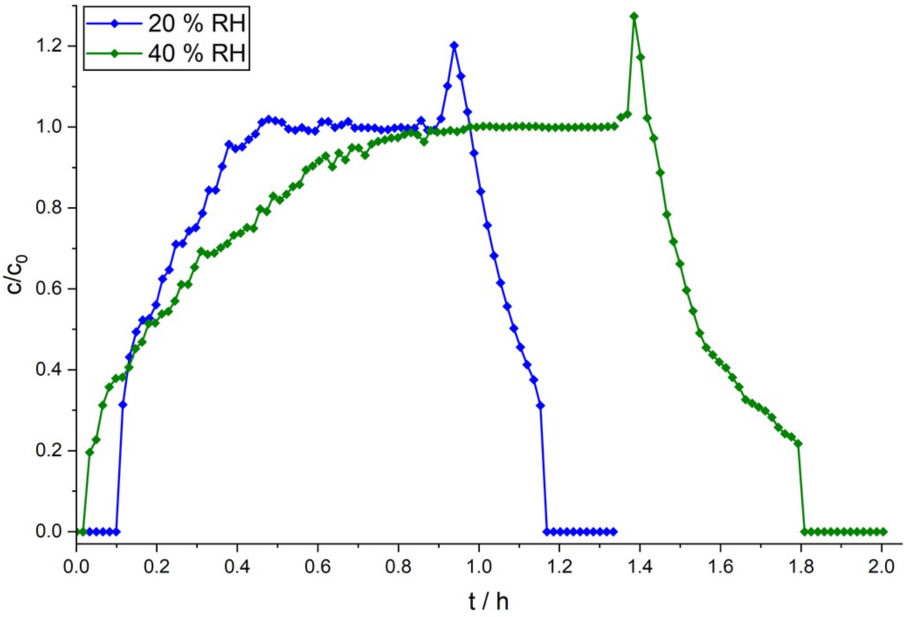

**Figure S3:** Breakthrough curves of the carbon foam with a helium gas stream with a 20 % RH (blue) and 40 % RH (green) at 25 °C at a flow rate of 110 sccm and a gas velocity of 0.01 m/s with a regeneration power of 0.5 W.

To show the reproducibility of the BT measurements using this setup, the water breakthrough curve of MOF-303@CF was measured three times independently at a relative humidity of 20 % and with 0.5 W of power for the joule heating assisted regeneration step (Figure S4). The curves show little deviations, especially in the adsorption branch, proving the high reproducibility of the experiment.

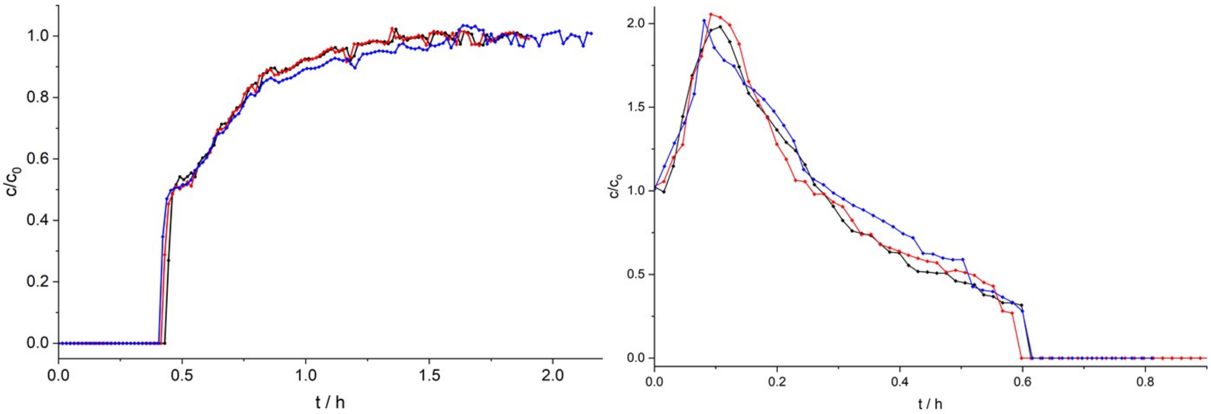

**Figure S4:** Comparison of three breakthrough measurements of MOF-303@CF to show the reproducibility. The measurement was done with a helium gas stream of 20 % RH at 25 °C at a flow rate of 110 sccm and a gas velocity of 0.01 m/s with a regeneration power of 0.5 W. The adsorption branches are shown on the left and the desorption on the right.

The water uptake from five breakthrough cycles at 40 % RH for MOF-303@CF was calculated and compared in figure S5 to show, that the material does not deteriorate and the water harvesting capacity remains constant even after several Joule-heating cycles.

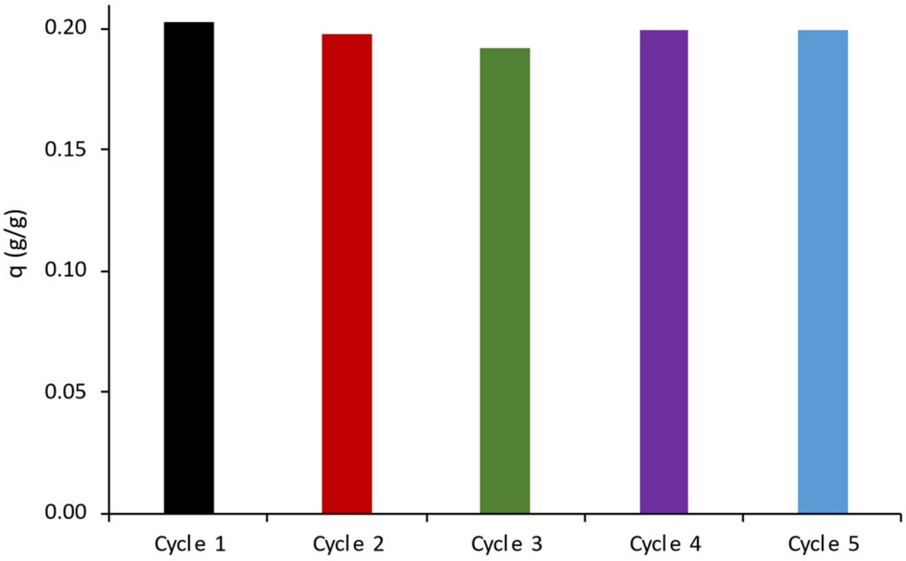

**Figure S5:** Comparison of the water uptake capacity of MOF-303@CF from five breakthrough cycles at 40 % RH.

## Characterization of the MOFs

To ensure optimal performance, the composition of the synthesized MOFs was verified by thermogravimetric and elemental analysis, the crystallinity and phase purity was confirmed by PXRD and the sorption characteristics were checked via nitrogen sorption at 77 K.

**CAU-10-H:** [Al($C_8O_4H_4$]

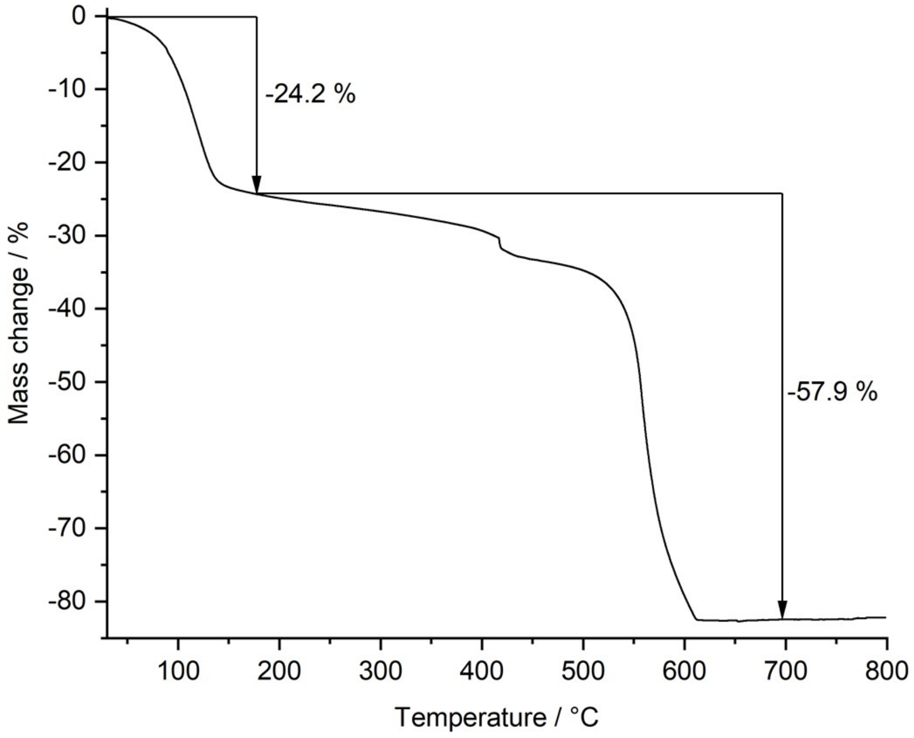

**Figure S6:** TG curve of CAU-10-H.

**Table S1:** Determination of the composition of CAU-10-H.

| | C % | H % | N % | S % | Solvent step % | Frame step % |
|---|---|---|---|---|---|---|
| Experimental | 33.94 | 4.65 | 0 | 0 | 24.2 | 57.9 |
| [AlOH($C_8H_4O_4$]x3.7 $H_2O$ | 34.97 | 4.55 | 0 | 0 | 24.3 | 57.2 |

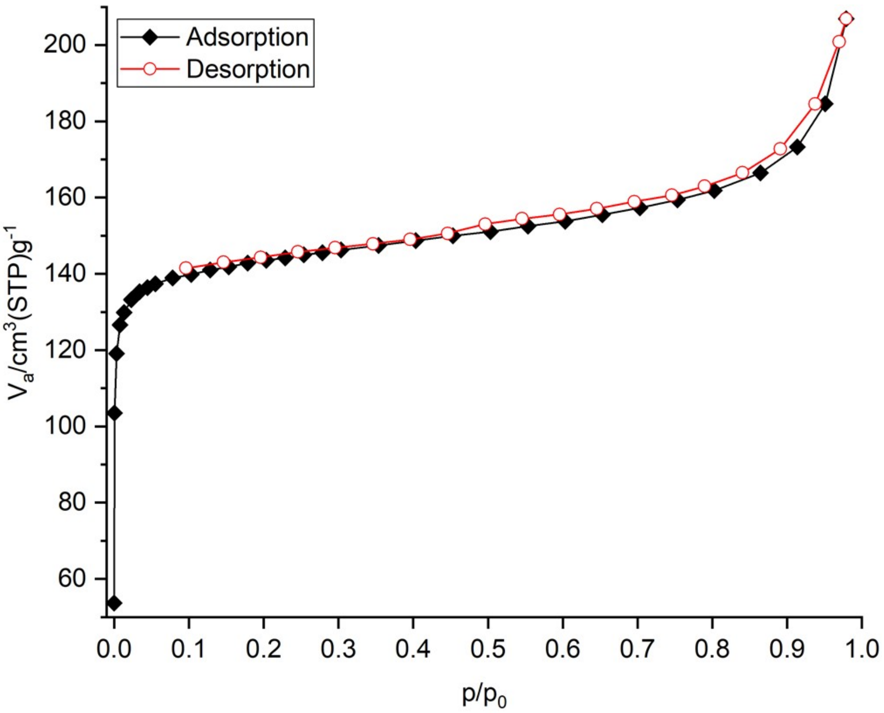

**Figure S7:** Nitrogen sorption isotherm of CAU-10-H at 77 K. The specific BET surface area calculated using the Rouquerol method is 571 m$^2$/g.

**MOF-303:** [$Al(C_5N_2O_4H_2)(OH)$]

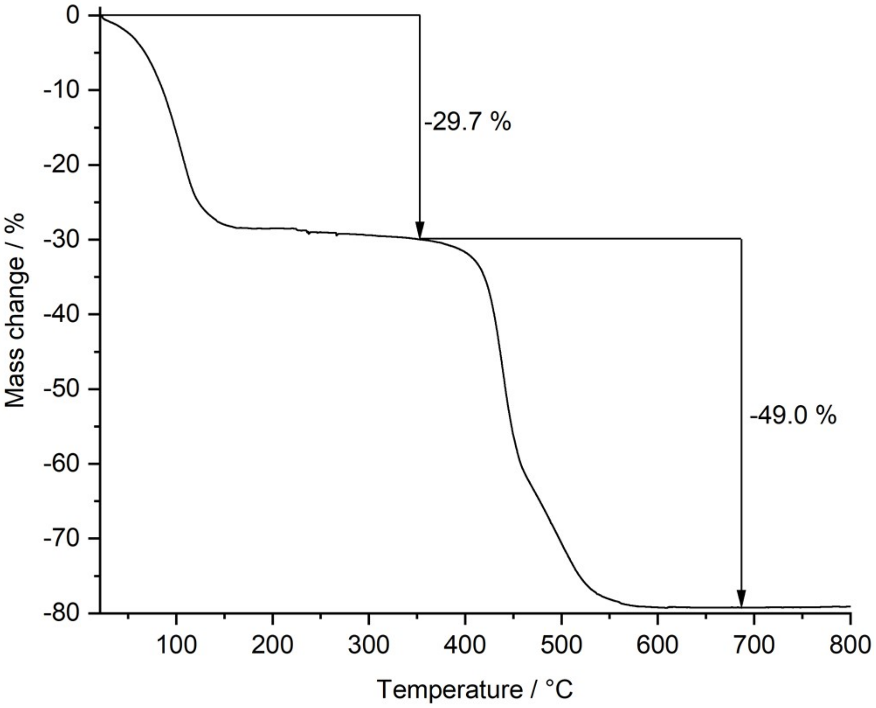

**Figure S8:** TG curve of MOF-303.

**Table S2:** Determination of the composition of MOF-303.

| | C % | H % | N % | S % | Solvent step % | Frame step % |
|---|---|---|---|---|---|---|
| Experimental | 21.18 | 4.55 | 9.68 | 0 | 29.7 | 49.0 |
| [$AlOH(C_5N_2H_2O_4)$]x4.7 $H_2O$ | 21.24 | 4.42 | 9.91 | 0 | 30.0 | 52.0 |

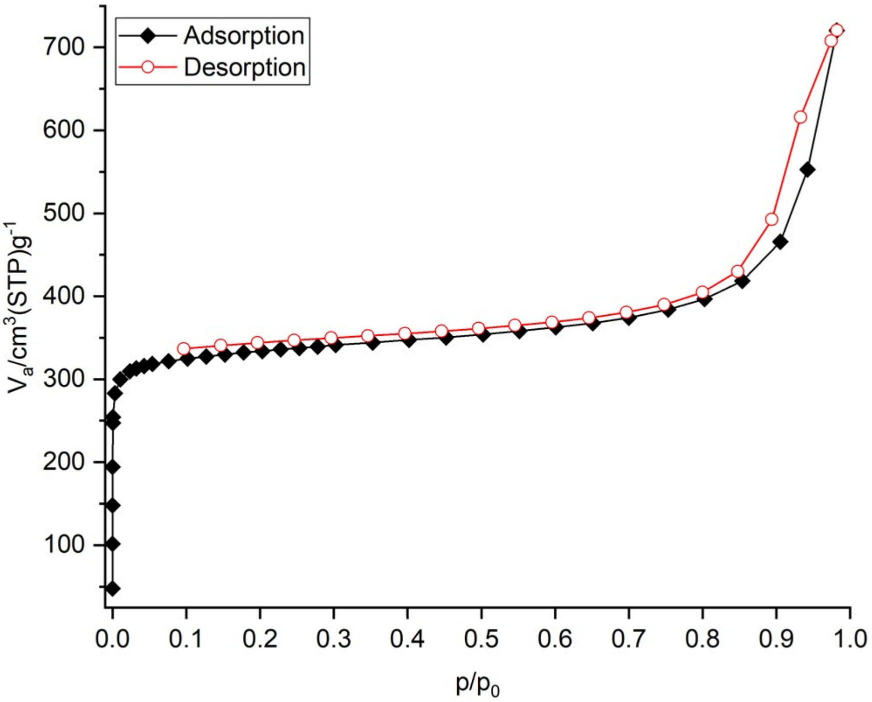

**Figure S9:** Nitrogen sorption isotherm of MOF-303 at 77 K. The specific BET surface area calculated using the Rouquerol method is 1322 $m^2/g$.

**MOF-801:** $[Zr_6O_4(OH)_4(C_4H_2O_4)_6]$

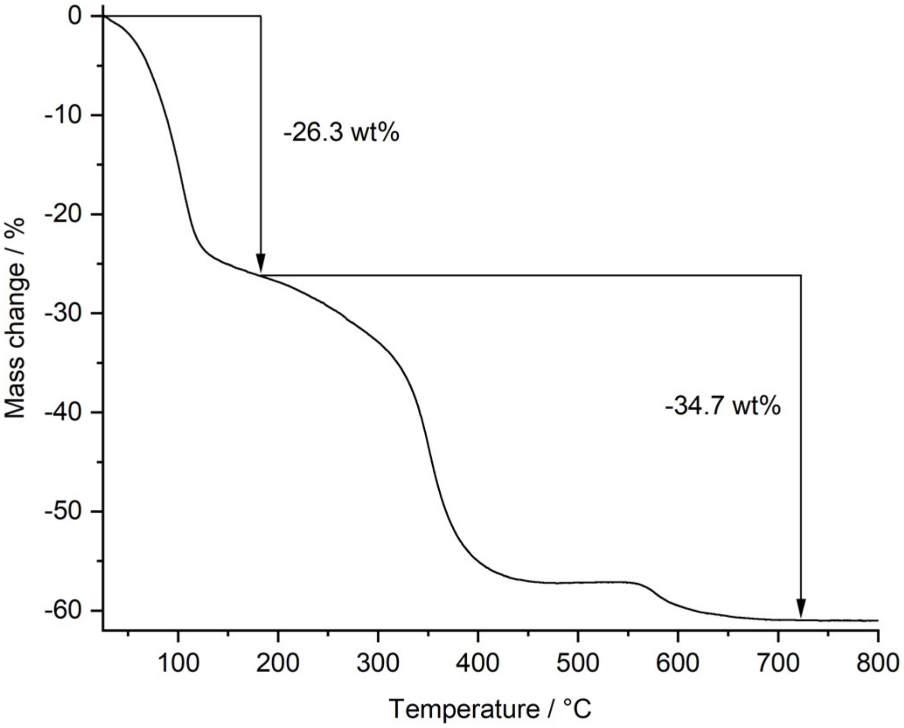

**Figure S10:** TG curve of MOF-801.

**Table S3:** Determination of the composition of MOF-801.

| | C % | H % | N % | S % | Solvent step % | Frame step % |
|---|---|---|---|---|---|---|
| Experimental | 15.65 | 4.07 | 0 | 0 | 26.3 | 34.7 |
| $[Zr_6O_4(OH)_4(C_4H_2O_4)_6]$x27 $H_2O$ | 15.58 | 3.81 | 0 | 0 | 26.3 | 33.8 |

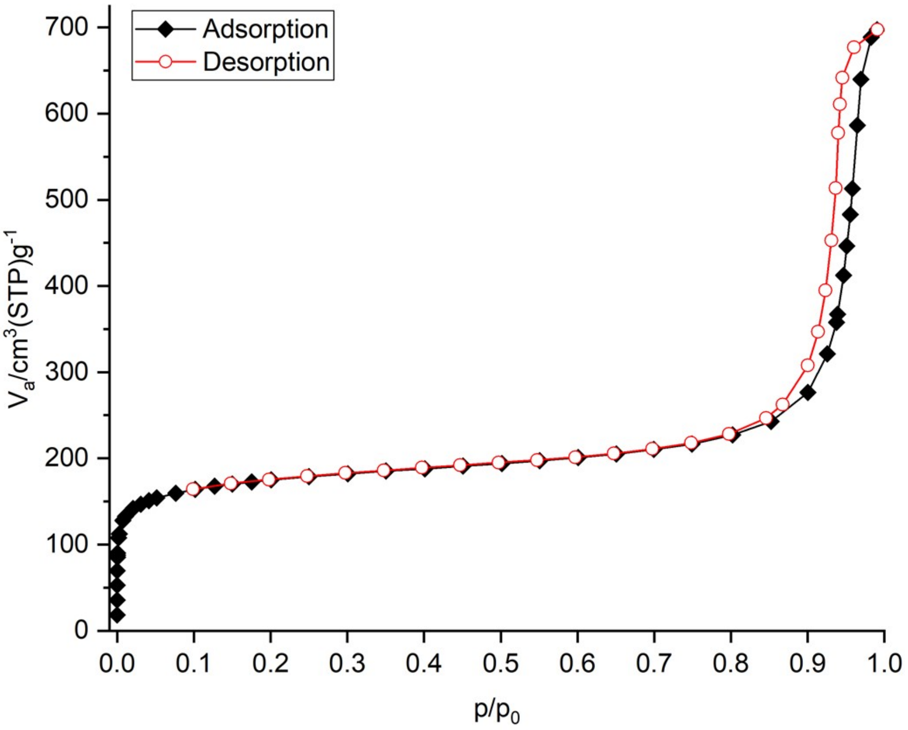

**Figure S11:** Nitrogen sorption isotherm of MOF-801 at 77 K. The specific BET surface area calculated using the Rouquerol method is 641 $m^2/g$.

## Characterization of the carbon foam

To understand the influence of the carbon substrate on the properties of the final composites, also the carbon foam was analysed via thermogravimetric and elemental analysis and additionally water sorption isotherms at 298 K and nitrogen sorption isotherms at 77 K were collected.

Elemental analysis: C: 62.107 %, H: 2.12 %, N: 8.05 %, S: 0.46 %

The remaining 27.2 % are likely made up by oxygen from the adsorbed water molecules and to a smaller part by sodium, which is present in the Basotect® W polymer in the form of sodium bisulfite.[1] EDX measurements confirmed the presence of sodium in the carbon foam even after the heat treatment and washing step.

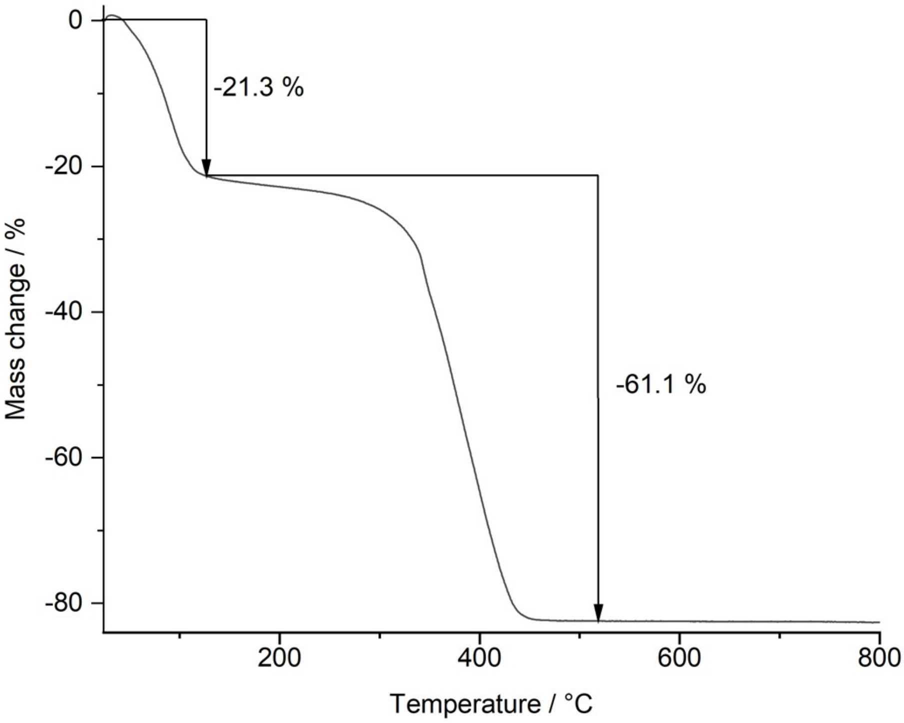

**Figure S12:** TG curve of the carbon foam.

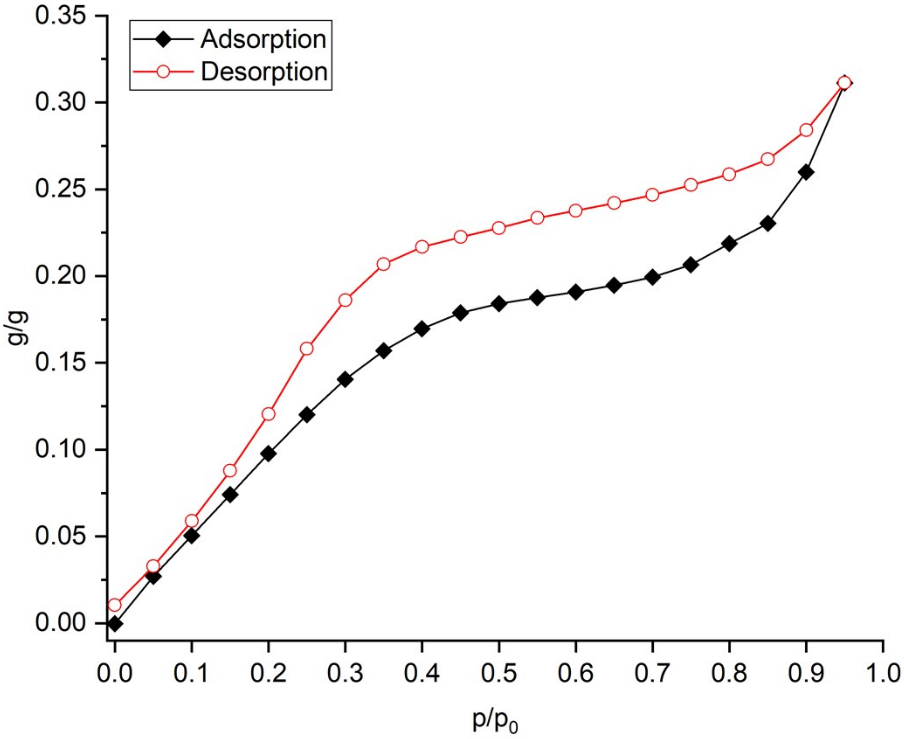

**Figure S13:** Water sorption isotherms of the carbon foam collected at 25 °C.

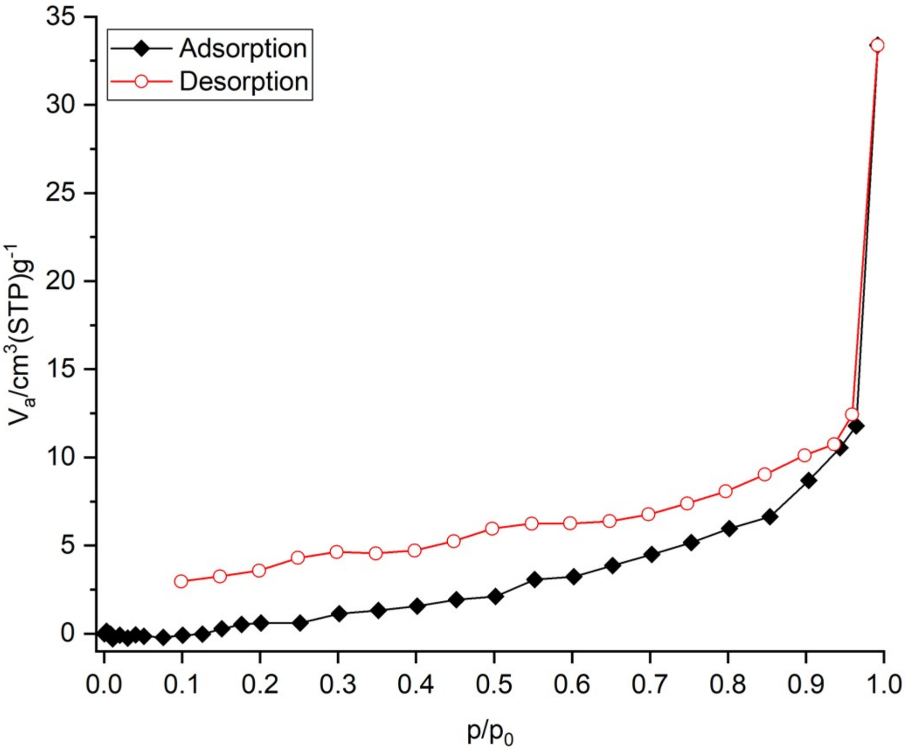

**Figure S14:** Nitrogen sorption isotherms of the carbon foam collected at 77 K.

## Powder X-ray diffraction

PXRD patterns of the composites were collected and compared to the respective MOF powders, to prove, that the material stays intact after the infiltration process.

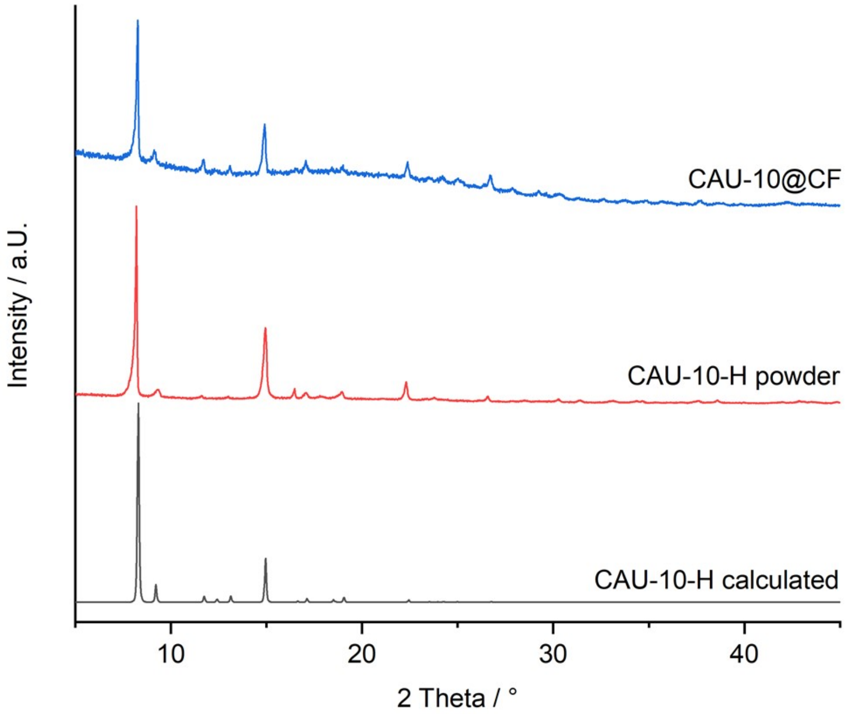

**Figure S15:** Powder diffraction patterns of CAU-10-H and CAU-10@CF compared with the simulated pattern.[2]

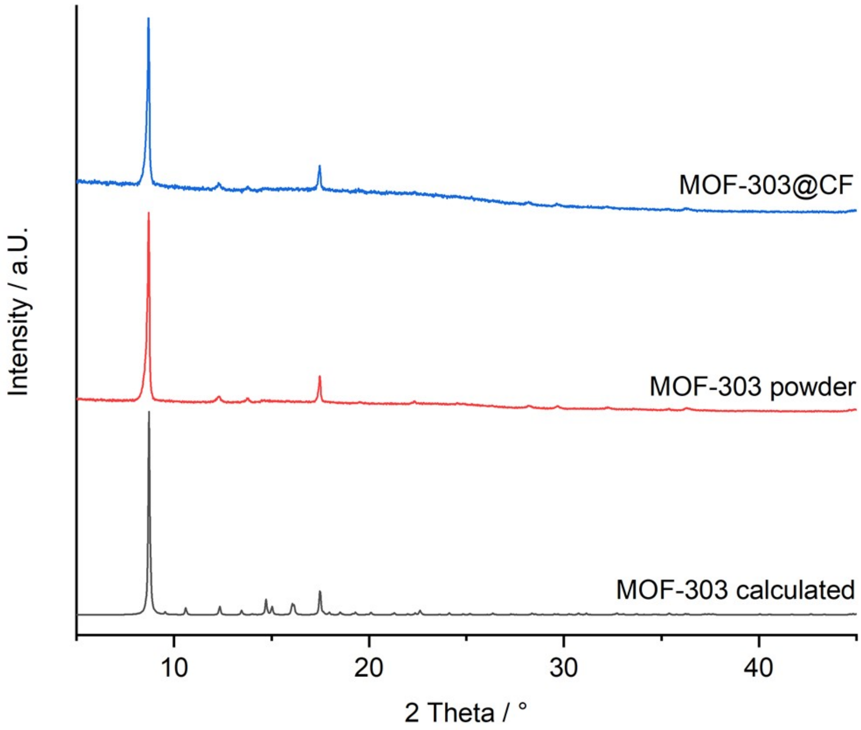

**Figure S16:** Powder diffraction patterns of MOF-303 and MOF-303@CF compared with the simulated pattern.[3]

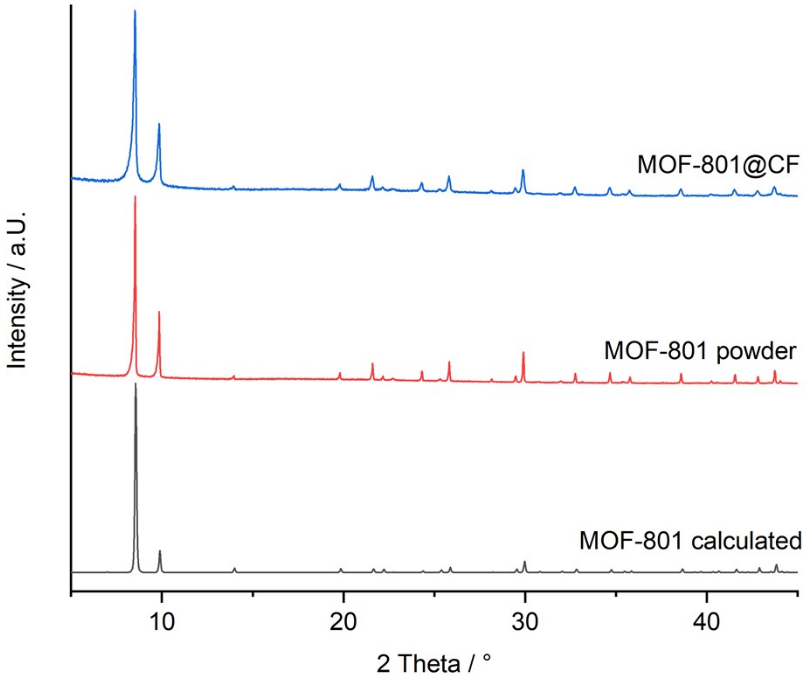

**Figure S17:** Powder diffraction patterns of MOF-801 and MOF-801@CF compared with the simulated pattern.[4]

## Dynamic light scattering and zeta-potential measurements

To obtain the hydrodynamic particle sizes and particle size distributions of the MOF crystallites, dynamic light scattering measurements were conducted in aqueous dispersions of the respective MOF.

**Table S4:** Hydrodynamic radius $d_{h,}$ polydispersity index PDI and zeta-potential of the three MOF particles measured in an aqueous dispersion.

| | CAU-10-H | MOF-303 | MOF-801 |
|---|---|---|---|
| $d_h$ [nm] | 211.0 ± 527.5 | 232.6 ± 139.0 | 57.9 ± 23.4 |
| PDI | 0.8 | 0.2 | 0.2 |
| Zeta potential [mV] | 16.92 | 20.97 | 22.75 |

## Light emission spectrum

To explore solar irradiation as an alternative regeneration pathway, the composites were irradiated with white light at different powers. The emission spectrum of the light source that was used is shown in Figure S17.

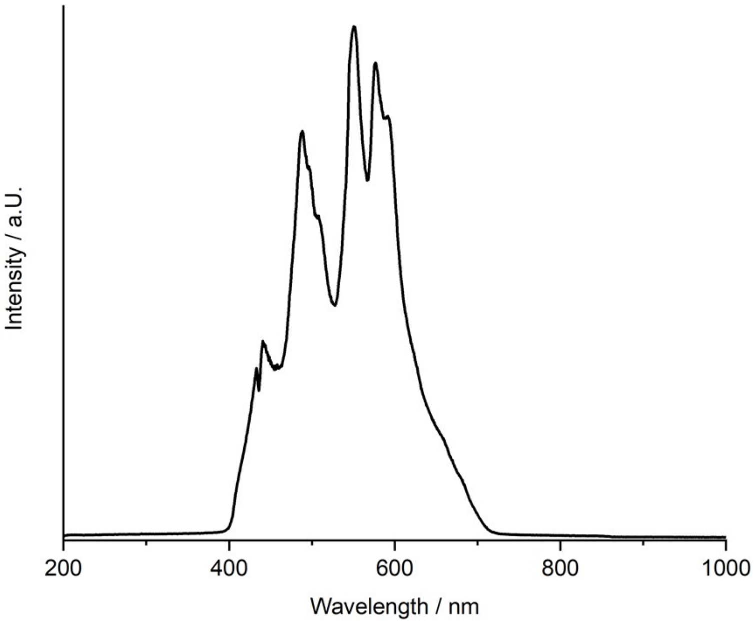

**Figure S18:** Emission spectrum of the light source that was used for the photonic heating of the composite materials.

## Heating experiments

To assess the heating behaviour of the composites, the time dependent temperature response after heating with different electrical and radiative powers was recorded (Figure S18-19). The power input trough light irradiation was measured using a thermal power sensor, considering the surface area of the composites.

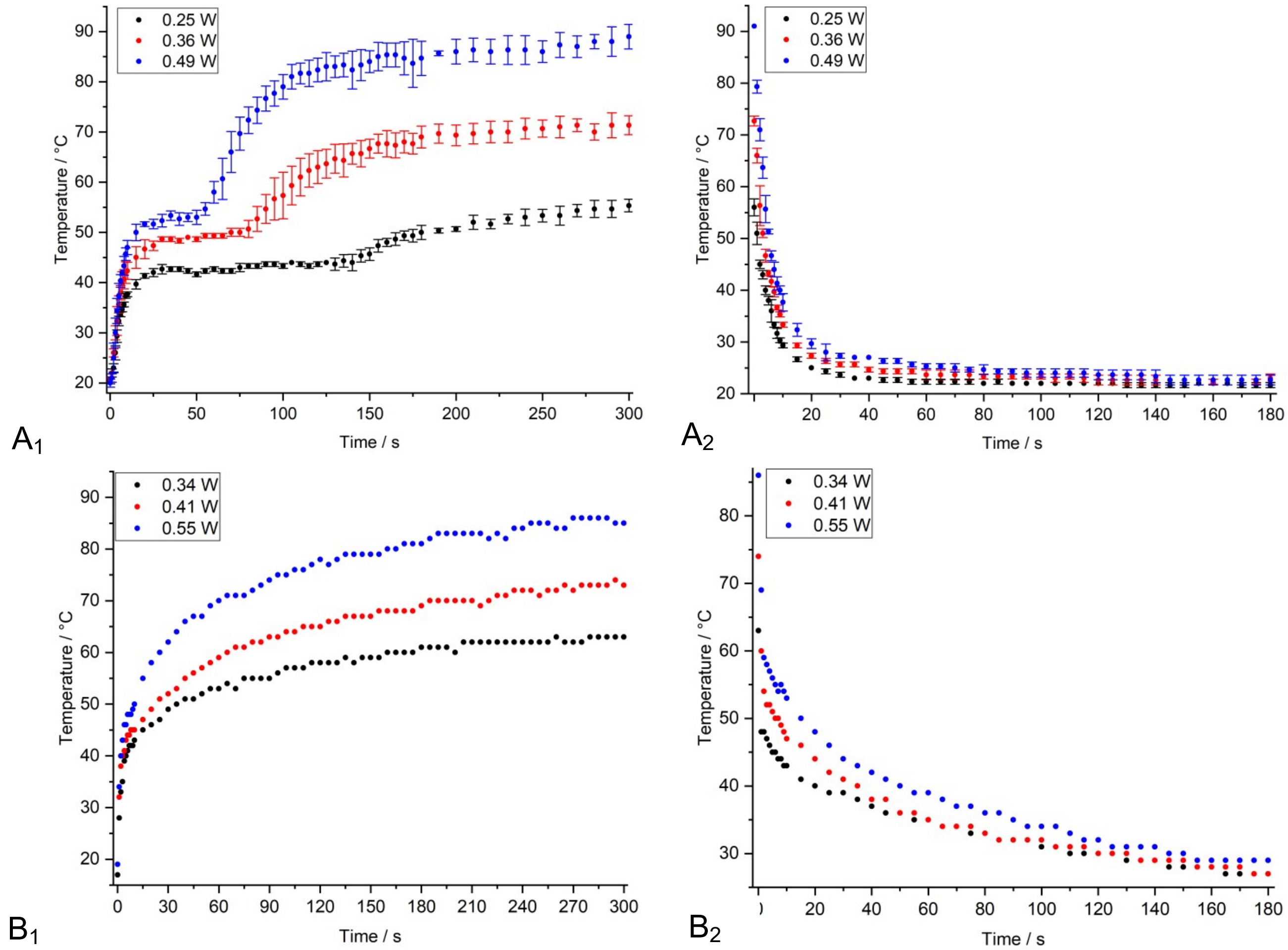

**Figure S19:** Joule-heating and cooling curves of CAU-10@CF shown in $A_1$ and $A_2$ respectively compared with the heating and cooling curves for radiative heating shown in $B_1$ and $B_2$.

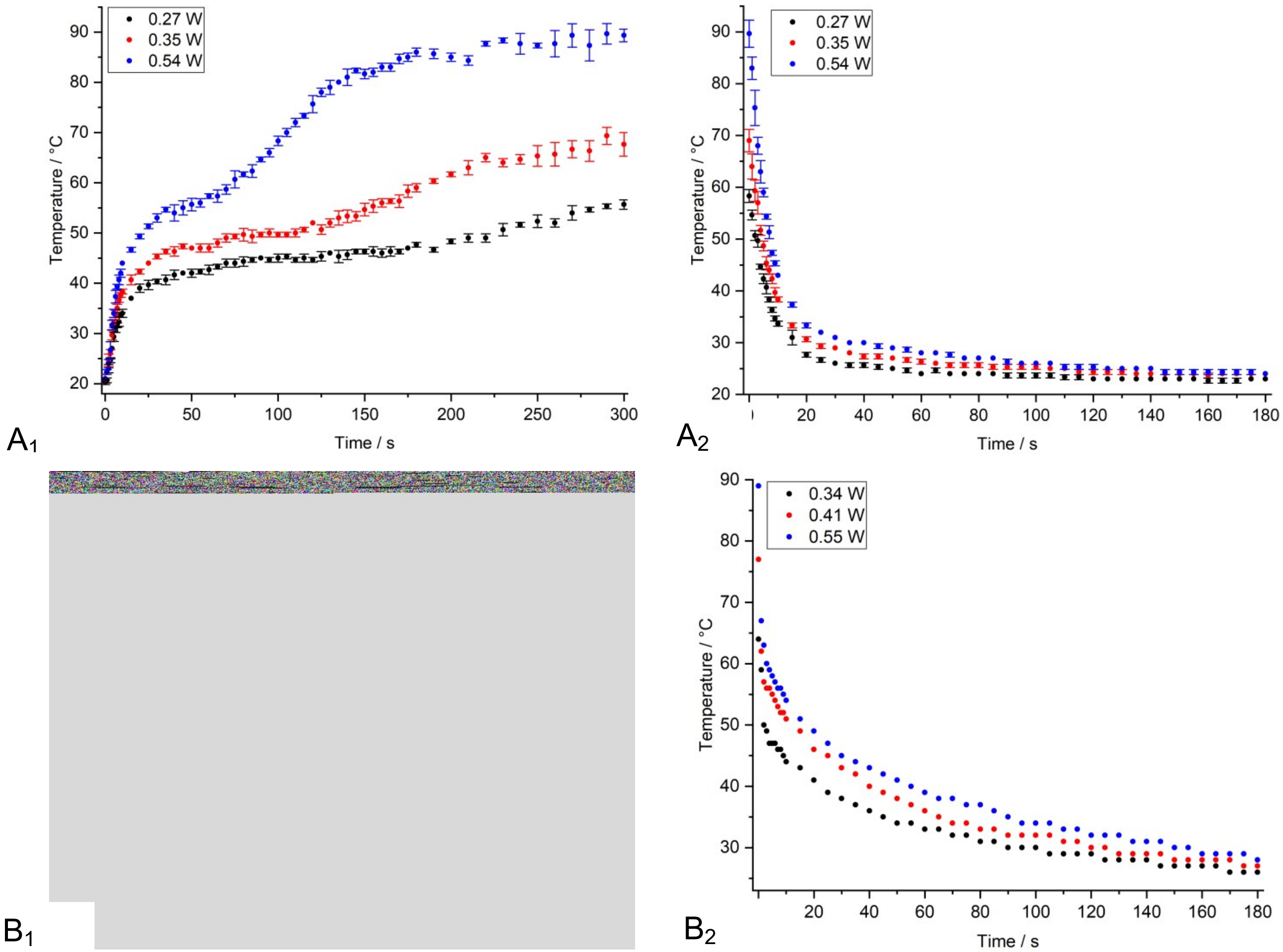

**Figure S20:** Joule-heating and cooling curves of MOF-303@CF shown in A$_1$ and A$_2$ respectively compared with the heating and cooling curves for radiative heating shown in B$_1$ and B$_2$.

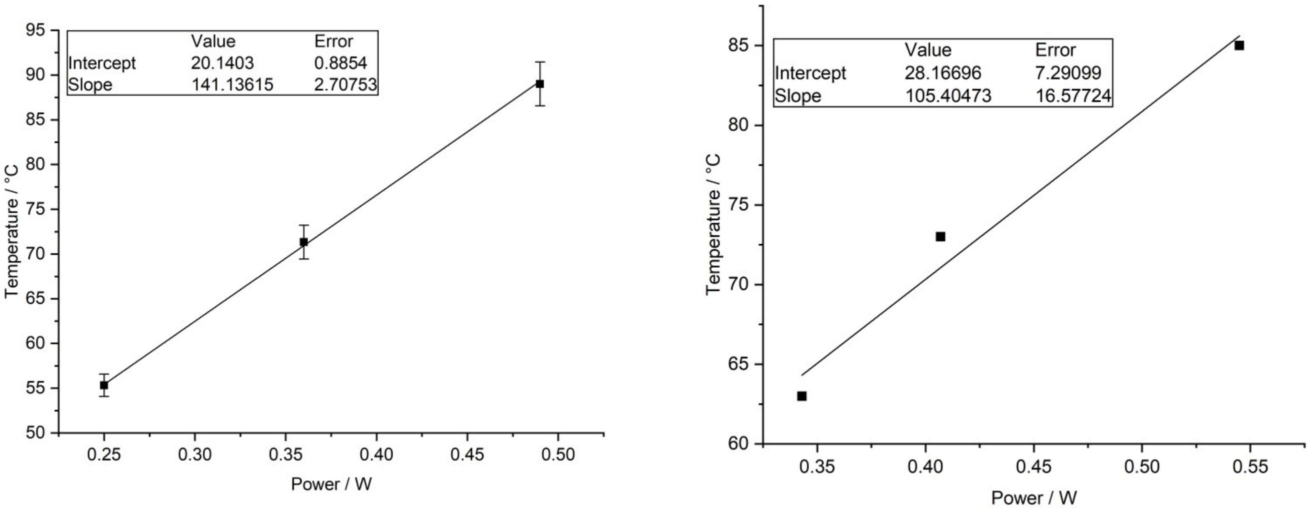

**Figure S21:** Linear regression for the temperature as function of the joule- (left) and radiative (right) heating power for CAU-10@CF.

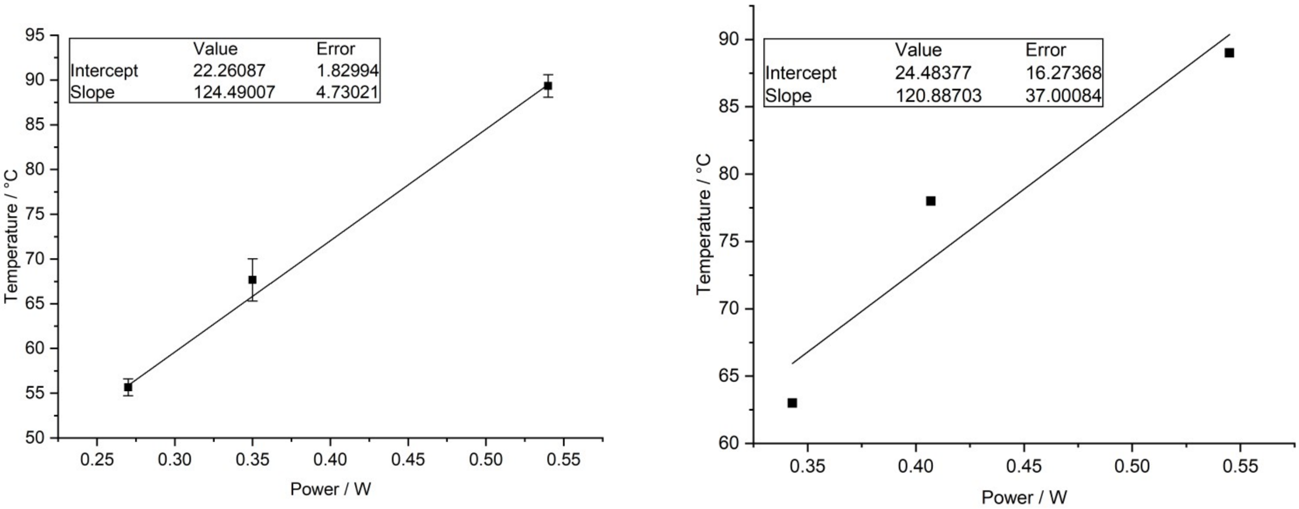

**Figure S22:** Linear regression for the temperature as function of the joule- (left) and radiative (right) power for MOF-303@CF.

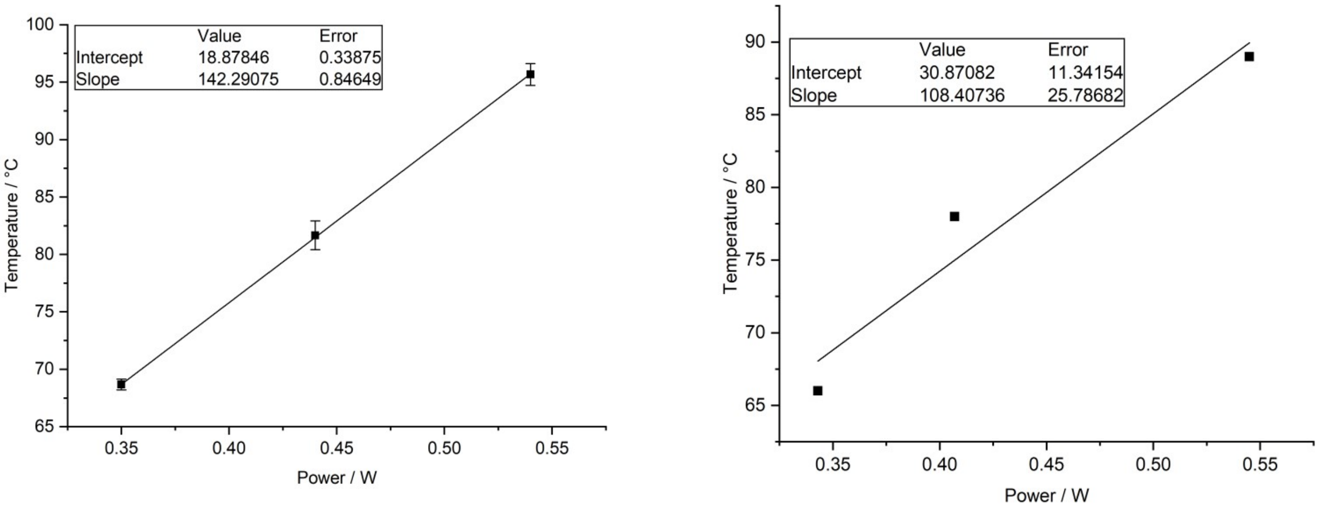

**Figure S23:** Linear regression for the temperature as function of the joule- (left) and radiative (right) power for MOF-801@CF.

## Calculations of the energy consumption

To understand the power needed to produce water from the composites through joule heating, the energy demand per litre of water produced at different regeneration conditions was calculated. The calculations in table S5 only take the power needed to desorb the water from the composite through joule-heating into consideration and not the potentially required energy for running a fan and a condensation unit. The energy consumption $E$ of our devices is calculated as the product of the desorption time $t$, the Joule-heating power $P$ and the scale factor $S$ :

$$E = t \cdot P \cdot S \tag{7}$$

The scale factor represents the number of times the measured composites would need to be multiplied to desorb 1 L (1000 g) of water in one sorption cycle and is calculated using the adsorption capacity $c$ and the mass of the composites $m(g)$as follows:

$$S = \frac{1000\, g}{c\, m(g)} \tag{8}$$

Since the desorption proceeds faster at the beginning of the regeneration step, it is more energetically efficient to only partly regenerate the adsorbent instead of waiting until all water is desorbed, at the cost of lowered daily water production (Table S3). Thus, the optimal operation conditions for running the AWH device change based on the water needs and the power availability.

Due to the small scale of the devices tested in this study, the scale factor needed for realizing these water yields is higher than 50 000, making a linear scalability unlikely. Thus, these values can only be seen as a rough upper limit to the possible power consumption of such a device for producing water on the litre scale. To further reduce the power consumption in future iterations of water harvesting devices, regeneration with lower electrical power or in heating pulses instead of applying a continuous current could be explored.

**Table S5:** Calculated power consumption for producing water from the composites through joule heating at different regeneration conditions.

| | 100 % regeneration with 0.5 W | | 50 % regeneration with 0.5 W | | 75 % regeneration with 0.5 W | |
|---|---|---|---|---|---|---|
| | Power demand [kWh/L$_{H2O}$] | Daily yield [L/(kg d)] | Power demand [kWh/L$_{H2O}$] | Daily yield [L/(kg d)] | Power demand [kWh/L$_{H2O}$] | Daily yield [L/(kg d)] |
| CAU-10@CF 20 % RH | 39.6 | 1.05 | 27.8 | 0.67 | 30.4 | 0.91 |
| CAU-10@CF 40 % RH | 25.4 | 1.83 | 16.6 | 1.23 | 20.2 | 1.62 |
| MOF-303@CF 20 % RH | 24.5 | 1.98 | 14.6 | 1.33 | 16.3 | 1.81 |
| MOF-303@CF 40 % RH | 20.9 | 2.18 | 12.8 | 1.43 | 14.8 | 1.95 |
| MOF-801@CF 20 % RH | 27.0 | 1.57 | 21.0 | 1.0 | 22.1 | 1.37 |
| MOF-801@CF 40 % RH | 21.7 | 1.45 | 15.0 | 0.88 | 16.0 | 1.24 |

The minimal energy requirement $E(min)$ for the water desorption can be calculated by considering the energy needed to heat the individual components (MOF, CF and water) to the desired desorption temperature of 70 °C and adding the energy for overcoming the enthalpy of adsorption of water on the respective adsorbents.

$$E(min) = E(heating, MOF) + E(heating, CF) + E\left(heating, H_2O\right) + E\left(des, H_2O\right) \quad (9)$$

For the sake of simplicity, the water is assumed to be completely adsorbed in the MOFs and not in the carbon foam. The specific heat capacities $C_P$ at 25 °C for the MOFs are 1.3 J/(g·K)[5], 1.0 J/(g·K)[6] and 0.8 J/(g·K)[7] for CAU-10-H, MOF-303 and MOF-801 respectively and assumed to be constant in the temperature range up to 70 °C. For the carbon foam, the specific heat capacity of graphite (0.7 J/(g·K)[8]) is assumed, while water has a heat capacity of 4.2 J/(g·K). The average heat of adsorption $\Delta H_{Ads}$ for water in the three MOFs is very similar, with -56 kJ/mol (CAU-10-H)[5], -54 kJ/mol (MOF-303)[9] and -55 kJ/mol (MOF-801).[7] To calculate the energy needed to desorb one liter of water, the mass of composite necessary to adsorb one liter of water can be calculated using the water harvesting capacity of the composites:

$$m(g) = \frac{1000\,g}{c} \quad (10)$$

Knowing that the composites contain a MOF mass fraction of 73 % and that the temperature difference from 25 °C to 70 °C is 45 K, the minimal power requirement to desorb one liter of water (55.6 mol) from each composite can be calculated as follows:

$$\begin{aligned} E(min) & \\ &= m(g) \cdot 0.73 \cdot C_P(MOF) \cdot 45\,K + m(g) \cdot 0.27 \cdot C_P(CF) \cdot 45\,K + 1000\,g \cdot C_P\left(H_2O\right) \cdot 45\,K \\ &\cdot 55.6\,mol \end{aligned} \quad (11)$$

This results in an energy requirement of 1.0 kWh, 0.94 kWh and 0.96 kWh for CAU-10@CF, MOF-303@CF and MOF-801@CF respectively. The values are very similar, since the adsorption enthalpy, which is very close in all three MOFs, is the dominating energy contributor. These values are significantly lower, than the reported energy consumption, signaling, that the reported devices have a large amount of systemic energy losses due to factors like internal resistance and heat loss to the environment. Future iterations of this technology should therefore focus on the device engineering to minimize this discrepancy.

**Literature comparison**

To compare the water harvesting results obtained in this study to the state of the art, a literature search using the terms "MOF" and "Atmospheric water harvesting" was conducted using Web of Science. Only studies that used MOFs as active materials and reported daily water yields per kg of adsorbent in the humidity range of 20 % to 40 % were considered for the comparison. The materials are ranked based on their daily water harvesting capacity and presented together with other relevant AWH parameters in Table S6. Since only few studies report the energy efficiency of the water harvesting devices, column 4 (energy use) contains only few entries. The ranking shows that while the water production capacities of the presented materials are not record-breaking, they show competitive performance compared to the overall literature. Due to the limited amount of datapoints available, the energy consumption is difficult to compare but among the studies that did report this, the devices in the present study have an above average energy consumption. Overall, it has to be noted that the direct comparability of the listed materials can be somewhat misleading, since the employed mass and shape of the adsorbents varies widely as do experimental parameters like the speed of the airflow and the regeneration conditions. To ensure comparability standardized testing conditions should be used, including aspects such as sample weight, regeneration power, air flow speed, relative humidity and adsorption temperature.

**Table S6:** Comparison of the water harvesting capacities of MOF based water harvesting materials operating in the relative humidity range from 20 % to 40 %.

| Material | Water harvesting capacity [L/(kg d)] | RH [%] | Energy use [kWh/L] | Average cycle time [h] | T [°C] | Heating method | Form of the adsorbent | Ref. |
|---|---|---|---|---|---|---|---|---|
| **OM-UiO-66-NH** | 27.8 | 30 | Not reported | 0.25 | 25 | Simulated sunlight | Thin layer | [10] |
| **MOF-801** | 12.5 | 39 | Not reported | 0.4 | 24 | Hot air | Fluidized powder | [11] |
| **Fluorophenyl oligomer incorporated MOF** | 10.1 | 25 | Not reported | 0.5 | 25 | Simulated sunlight | Monolith | [12] |
| **Chitosan-hyaluronic acid-MOF-303-graphene oxide-calcium chloride composite** | 10.0 | ≈25 | 1.2-44.4 | Not reported | ≈30 | Simulated sunlight | Monolith | [13] |
| **MOF-303@poly(acrylates)** | 7.9 | 20 | Not reported | No reported | 25 | Electrical heater + vacuum | Beads | [14] |
| **TMM-MOF801** | 6.1 | 20 | Not reported | 0.7 | 25 | Joule-heating | Membrane | [15] |
| **MOF-AG@IO** | 6.0 | 33 | 89.1 | 1 | 25 | Induction | Beads | [16] |
| **Photothermal-triggered MOF-composite nanofiber texture** | 4.6 | 23 | Not reported | 4.8 | 34 | Simulated sunlight | Fibers | [17] |
| **Octahedral nitrogen-modified MOF-80** | 4.6 | 30 | Not reported | 0.7 | 25 | Simulated sunlight | Powder | [18] |
| **MIL-101(Cr) monolith** | 3.7 | 30 | Not reported | 2 | 25 | Peltier effect | Monolith | [19] |
| **MOF-801** | 1.8-3.5 | 19-46 | 1.7-5.3 | From 4 to 0.8 | ≈25 | Electric heater | Powder | [20] |
| **MOF-303@CF** | **2.2** | **40** | **20.9** | **2.2** | **25** | **Joule-heating** | **Monolith** | **This work** |

| | | | | | | | | |
|---|---|---|---|---|---|---|---|---|
| **MOF-303@CF** | **2.0** | **20** | **24.5** | **1.7** | **25** | **Joule-heating** | **Monolith** | **This work** |
| **Al-fum-carbon scaffold** | 2.0 | 28-38 | 1.6 | 2.5 | 23-26 | Joule-heating | Monolith | [21] |
| **MOF-Based Zwitterionic Hydrogel** | 1.9 | 20-40 | 0 | 24 | 20-32 | Sunlight | Monolith | [22] |
| **CAU-10@CF** | **1.8** | **40** | **25.4** | **2.2** | **25** | **Joule-heating** | **Monolith** | **This work** |
| **$Ti_3C_2$/sHBP-coated MOF** | 1.8 | 35 | 1.0 | 3 | 25 | Solar+electric heater | Monolith | [23] |
| **$Ni_2Cl_2$(BTDD) on Cu foam** | 1.8 | 35 | Not reported | 2.2 | 25 | Peltier effect | Monolith | [24] |
| **$CaCl_2$@MOF-808** | 1.8 | 30 | 0 | 2.7 | 25 | Sunlight | Powder | [25] |
| **CF/Al-fumarate/SA** | 1.7 | 32-35 | 4.4 | 3.3 | 26-28 | Joule-heating | Monolith | [26] |
| **MOF-801@CF** | **1.6** | **20** | **27.0** | **0.8** | **25** | **Joule-heating** | **Monolith** | **This work** |
| **MOF-801@P(NIPAM-GMA)** | 1.6 | 20 | Not reported | 3 | 25 | Electric heater + vacuum | Beads | [27] |
| **MOF-801@CF** | **1.5** | **40** | **21.7** | **2.5** | **25** | **Joule-heating** | **Monolith** | **This work** |
| **MOF-801 sodium alginate-tannic acid matrix** | 1.4 | 20 | Not reported | 2 | 26 | Simulated sunlight | Monolith | [28] |
| **WCBs@SA/MNPs/MOFs** | 1.4 | 20 | Not reported | 3 | 25 | Simulated sunlight | Monolith | [29] |
| **Carbon paper/MOF monolith** | 1.4 | 33-43 | 2.3 | 2.7 | 23-26 | Solar and joule-heating | Monolith | [30] |
| **MOF-303** | 1.3 | 32 | Not reported | 2-3 | 27 | Electrical heater | Powder | [31] |
| **D-Al-Fum** | 1.2 | 30 | Not reported | 3 | 25 | Electric heater | Powder | [32] |
| **CAU-10@CF** | **1.1** | **20** | **39.6** | **3.0** | **25** | **Joule-heating** | **Monolith** | **This work** |
| **MXene $Ti_3C_2$-incorporated UiO-66-$NH_2$ monolith** | 0.4 | 20 | Not reported | 1 | 25 | Simulated sunlight | Monolith | [33] |
| **MOF-801** | 0.3 | 20-40 | Not reported | 24 | 15-25 | Concentrated sunlight | Powder | [34] |
| **MOF-801@MIL-101(Cr)** | 0.3 | 10-20 | Not reported | 24 | 25 | Simulated sunlight | Powder | [35] |
| **MOF-303** | 0.1-0.3 | 9.4-36 | 0 | 24 | 22-61 | Sunlight | Pellets | [36] |
| **MOF-801** | 0.1 | 20-40 | 0 | 24 | 15-25 | Sunlight | Powder | [34] |

## References

1 H. Mahnke, F. P. Woerner, H. Weber, G. Kreibiehl, US Pat., US4540717A.

2 D. Fröhlich, E. Pantatosaki, P. D. Kolokathis, K. Markey, H. Reinsch, M. Baumgartner, M. A. van der Veen, D. E. De Vos, N. Stock, G. K. Papadopoulos, S. K. Henninger and C. Janiak, *J. Mater. Chem. A*, 2016, **4**, 11859–11869.

3 N. Hanikel, X. Pei, S. Chheda, H. Lyu, W. Jeong, J. Sauer, L. Gagliardi and O. M. Yaghi, *Science*, 2021, **374**, 454–459.

4 H. Furukawa, F. Gándara, Y.-B. Zhang, J. Jiang, W. L. Queen, M. R. Hudson and O. M. Yaghi, *J. Am. Chem. Soc.*, 2014, **136**, 4369–4381.

5 D. Fröhlich, E. Pantatosaki, P. D. Kolokathis, K. Markey, H. Reinsch, M. Baumgartner, M. A. van der Veen, D. E. de Vos, N. Stock, G. K. Papadopoulos, S. K. Henninger and C. Janiak, *J. Mater. Chem. A*, 2016, **4**, 11859–11869.

6 A. E. Abu El-maaty, O. Saoudi, A. S. Abdelrazik and R. Ben-Mansour, *International Communications in Heat and Mass Transfer*, 2025, **165**, 109088.

7 H. Kim, S. Yang, S. R. Rao, S. Narayanan, E. A. Kapustin, H. Furukawa, A. S. Umans, O. M. Yaghi and E. N. Wang, *Science*, 2017, **356**, 430–434.

8 C. Yin, L. Ziru, W. Ganghe, W. Chengyun and others, *Proc. Int. Pyrotech. Semin. 17th*, 1991, **1**, 515–521.

9 Z. Zheng, N. Hanikel, H. Lyu and O. M. Yaghi, *J. Am. Chem. Soc.*, 2022, **144**, 22669–22675.

10 Z. He, Y. Liu, C. Wang, C. Lin, Z. Wang, W. Kuang, G. Zeng, C. Wang, F. Wang, B. Liu, L. Zhang, A. Baqais, S. Rouf, S. A. Zuhair, Y. Greish, M. A. Alhussaini, A. S. Alquwaizany, E. Almatrafi, W. Lu, Y. Shi, J. Cao, W. Wang and P. Wang, *Small*, 2026, e73429.

11 A. Terzis, A. Ramachandran, K. Wang, M. Asheghi, K. E. Goodson and J. G. Santiago, *Cell Rep. Phys. Sci.*, 2020, **1**, 100057.

12 M. S. Kang, I. Heo, S. H. Park, J. Bae, S. Kim, G. Kim, B.-H. Kim, N. C. Jeong and W. C. Yoo, *Nat. Commun.*, 2024, **15**, 9793.

13 Q. Luo, T. Zhang, M. Chen, C. Gao, L. Guo, M. Zhou, L. Zhu, H. Wei, A. Khan, Y. Hou and Y. Zheng, *Small*, 2025, **21**, e2503948.

14 M. Li, S. Xu, J. Liang, H. Meng, G. Xiang, J. Mi, J. Jin and J. Liu, *Nano Research*, 2026, **19**, 94908458.

15 Y. Tao, J. Sun, Q. Wu, D. Zhu and H. Li, *Chemical Engineering Journal*, 2023, **461**, 141864.

16 R. Sharma, G. Saab, M. Schoukens, T. R. van Assche and J. F. Denayer, *Appl. Mater. Today*, 2023, **35**, 101918.

17 D. Yu, X. Han, S. Wang, L. Zhong, L. Zhang, M. Zhou, Q. Luo, T. Zhang, L. Zhu, Y. Hou and Y. Zheng, *Sep. Purif. Technol.*, 2024, **331**, 125629.

18 X. Yan, F. Xue, C. Zhang, H. Peng, J. Huang, F. Liu, K. Lu, R. Wang, J. Shi, N. Li, W. Chen and M. Liu, *EcoMat*, 2024, **6**.

19 Y. Tao, B. Zhu, D. Zhu and H. Li, *Ind. Eng. Chem. Res.*, 2024, **63**, 13600–13610.

20 H. A. Almassad, R. I. Abaza, L. Siwwan, B. Al-Maythalony and K. E. Cordova, *Nat. Commun.*, 2022, **13**, 4873.

21 Y. Tao, Q. Wu, C. Huang, D. Zhu and H. Li, *Chemical Engineering Journal*, 2023, **451**, 138547.

22 H. Pan, L. Zhu, H. Wei, C. Gao, M. Zhou, T. Zhang, Q. Luo, B. Tian, J. Wang, Y. Hou and Y. Zheng, *Adv Materials Inter*, 2025, **12**.

23 Q. Wu, Z. Feng, X. Zhou and H. Li, *Ind. Eng. Chem. Res.*, 2024, **63**, 4866–4875.

24 Z. Chen, X. Yang, Z. Cui, S. Du and R. Wang, *Nano Energy*, 2024, **125**, 109596.

25 H. An, Y. Chen, Y. Wang, X. Liu, Y. Ren, Z. Kang, J. Li and L. Li, *Chemical Engineering Journal*, 2023, **461**, 141955.

26 Q. Li, Y. Ying, Y. Tao and H. Li, *Ind. Eng. Chem. Res.*, 2022, **61**, 1344–1354.

27 C. Yang, H. Wu, J. Yun, J. Jin, H. Meng, J. Caro and J. Mi, *Adv. Mater.*, 2023, **35**, e2210235.

28 M. Zhu, G. He, Z. Wang, J. Chen, X. Fu, H. Yang, P. Lyu, S. Gu, X. Liu and B. Shang, *Journal of Environmental Chemical Engineering*, 2024, **12**, 113815.

29 B. Shang, M. Zhu, Z. Wang, J. Chen, X. Fu, H. Yang, Z. Deng, P. Lyu, J. Du, D. Chen, S. Gu and X. Liu, *Sep. Purif. Technol.*, 2025, **363**, 132238.

30 Y. Tao, Q. Wu, C. Huang, W. Su, Y. Ying, D. Zhu and H. Li, *ACS Appl. Mater. Interfaces*, 2022, **14**, 10966–10975.

31 N. Hanikel, M. S. Prévot, F. Fathieh, E. A. Kapustin, H. Lyu, H. Wang, N. J. Diercks, T. G. Glover and O. M. Yaghi, *ACS Cent. Sci.*, 2019, **5**, 1699–1706.

32 Q. Fu, D. Liu, J. Yang, Y. Jin, Z. Sun, C. Liu, Y. Sun, C. Sun, Q. Wang and Q. Ma, *Green Chem.*, 2025, **27**, 2680–2688.

33 Q. Wu, W. Su, Q. Li, Y. Tao and H. Li, *ACS Appl. Mater. Interfaces*, 2021, **13**, 38906–38915.

34 H. Kim, S. R. Rao, E. A. Kapustin, L. Zhao, S. Yang, O. M. Yaghi and E. N. Wang, *Nat. Commun.*, 2018, **9**, 1–8.

35 Y. Hu, Y. Wang, Z. Fang, X. Wan, M. Dong, Z. Ye and X. Peng, *J. Mater. Chem. A*, 2022, **10**, 15116–15126.

36 W. Song, Z. Zheng, A. H. Alawadhi and O. M. Yaghi, *Nat Water*, 2023, **1**, 626–634.